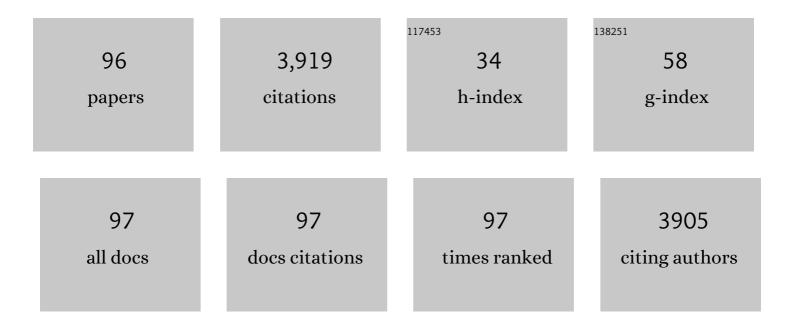
List of Publications by Year in descending order

Source: https://exaly.com/author-pdf/9406589/publications.pdf Version: 2024-02-01



#	Article	IF	CITATIONS
1	Polydopamine-filled bacterial nanocellulose as a biodegradable interfacial photothermal evaporator for highly efficient solar steam generation. Journal of Materials Chemistry A, 2017, 5, 18397-18402.	5.2	257
2	Advances in solar evaporator materials for freshwater generation. Journal of Materials Chemistry A, 2019, 7, 24092-24123.	5.2	190
3	Mechanically interlocked 1T/2H phases of MoS2 nanosheets for solar thermal water purification. Nano Energy, 2018, 53, 949-957.	8.2	156
4	Localized heating with a photothermal polydopamine coating facilitates a novel membrane distillation process. Journal of Materials Chemistry A, 2018, 6, 18799-18807.	5.2	138
5	Impacts of Geochemical Reactions on Geologic Carbon Sequestration. Environmental Science & Technology, 2013, 47, 3-8.	4.6	133
6	Cellulose Nanomaterials in Interfacial Evaporators for Desalination: A "Natural―Choice. Advanced Materials, 2021, 33, e2000922.	11.1	132
7	Dissolution and Precipitation of Clay Minerals under Geologic CO ₂ Sequestration Conditions: CO ₂ â^Brineâ^Phlogopite Interactions. Environmental Science & Technology, 2010, 44, 5999-6005.	4.6	120
8	Photothermal Membrane Water Treatment for Two Worlds. Accounts of Chemical Research, 2019, 52, 1215-1225.	7.6	117
9	Effects of Salinity and the Extent of Water on Supercritical CO ₂ -Induced Phlogopite Dissolution and Secondary Mineral Formation. Environmental Science & Technology, 2011, 45, 1737-1743.	4.6	89
10	A Robust and Scalable Polydopamine/Bacterial Nanocellulose Hybrid Membrane for Efficient Wastewater Treatment. ACS Applied Nano Materials, 2019, 2, 1092-1101.	2.4	89
11	The role of confined collagen geometry in decreasing nucleation energy barriers to intrafibrillar mineralization. Nature Communications, 2018, 9, 962.	5.8	86
12	Heterogeneous Nucleation and Growth of Nanoparticles at Environmental Interfaces. Accounts of Chemical Research, 2016, 49, 1681-1690.	7.6	83
13	In Situ Determination of Interfacial Energies between Heterogeneously Nucleated CaCO ₃ and Quartz Substrates: Thermodynamics of CO ₂ Mineral Trapping. Environmental Science & Technology, 2013, 47, 102-109.	4.6	78
14	In Situ Observations of Nanoparticle Early Development Kinetics at Mineralâ^'Water Interfaces. Environmental Science & Technology, 2010, 44, 8182-8189.	4.6	68
15	Interfacial Energies for Heterogeneous Nucleation of Calcium Carbonate on Mica and Quartz. Environmental Science & Technology, 2014, 48, 5745-5753.	4.6	68
16	A thermally engineered polydopamine and bacterial nanocellulose bilayer membrane for photothermal membrane distillation with bactericidal capability. Nano Energy, 2021, 79, 105353.	8.2	68
17	Hydrophilic, Bactericidal Nanoheater-Enabled Reverse Osmosis Membranes to Improve Fouling Resistance. ACS Applied Materials & Interfaces, 2015, 7, 11117-11126.	4.0	67
18	Polydopamine/hydroxyapatite nanowire-based bilayered membrane for photothermal-driven membrane distillation. Journal of Materials Chemistry A, 2020, 8, 5147-5156.	5.2	61

#	Article	IF	CITATIONS
19	Water Chemistry Impacts on Arsenic Mobilization from Arsenopyrite Dissolution and Secondary Mineral Precipitation: Implications for Managed Aquifer Recharge. Environmental Science & Technology, 2014, 48, 4395-4405.	4.6	60
20	Catalytically Active Bacterial Nanocelluloseâ€Based Ultrafiltration Membrane. Small, 2018, 14, e1704006.	5.2	59
21	Dissolved Organic Matter Affects Arsenic Mobility and Iron(III) (hydr)oxide Formation: Implications for Managed Aquifer Recharge. Environmental Science & Technology, 2019, 53, 14357-14367.	4.6	59
22	Heteroepitaxial Nucleation and Oriented Growth of Manganese Oxide Islands on Carbonate Minerals under Aqueous Conditions. Environmental Science & Technology, 2005, 39, 1239-1249.	4.6	58
23	Environmentally Abundant Anions Influence the Nucleation, Growth, Ostwald Ripening, and Aggregation of Hydrous Fe(III) Oxides. Langmuir, 2012, 28, 7737-7746.	1.6	57
24	Control of Heterogeneous Fe(III) (Hydr)oxide Nucleation and Growth by Interfacial Energies and Local Saturations. Environmental Science & Technology, 2013, 47, 9198-9206.	4.6	56
25	Photothermally Active Reduced Graphene Oxide/Bacterial Nanocellulose Composites as Biofouling-Resistant Ultrafiltration Membranes. Environmental Science & Technology, 2019, 53, 412-421.	4.6	56
26	NanoEHS – defining fundamental science needs: no easy feat when the simple itself is complex. Environmental Science: Nano, 2016, 3, 15-27.	2.2	53
27	Biotite–Brine Interactions under Acidic Hydrothermal Conditions: Fibrous Illite, Goethite, and Kaolinite Formation and Biotite Surface Cracking. Environmental Science & Technology, 2011, 45, 6175-6180.	4.6	50
28	Chemical Reactions of Portland Cement with Aqueous CO ₂ and Their Impacts on Cement's Mechanical Properties under Geologic CO ₂ Sequestration Conditions. Environmental Science & Technology, 2015, 49, 6335-6343.	4.6	50
29	Effects of Al/Si ordering on feldspar dissolution: Part I. Crystallographic control on the stoichiometry of dissolution reaction. Geochimica Et Cosmochimica Acta, 2014, 126, 574-594.	1.6	48
30	Achieving maximum recovery of latent heat in photothermally driven multi-layer stacked membrane distillation. Nano Energy, 2021, 80, 105444.	8.2	48
31	Aluminum Affects Heterogeneous Fe(III) (Hydr)oxide Nucleation, Growth, and Ostwald Ripening. Environmental Science & Technology, 2014, 48, 299-306.	4.6	43
32	Enhanced Colloidal Stability of CeO ₂ Nanoparticles by Ferrous Ions: Adsorption, Redox Reaction, and Surface Precipitation. Environmental Science & Technology, 2015, 49, 5476-5483.	4.6	39
33	Arsenic mobilization and attenuation by mineral–water interactions: implications for managed aquifer recharge. Journal of Environmental Monitoring, 2012, 14, 1772.	2.1	37
34	Photochemically assisted fast abiotic oxidation of manganese and formation of δ-MnO ₂ nanosheets in nitrate solution. Chemical Communications, 2017, 53, 4445-4448.	2.2	37
35	The apparent activation energy and pre-exponential kinetic factor for heterogeneous calcium carbonate nucleation on quartz. Communications Chemistry, 2018, 1, .	2.0	36
36	Wollastonite Carbonation in Water-Bearing Supercritical CO ₂ : Effects of Particle Size. Environmental Science & Technology, 2017, 51, 13044-13053.	4.6	35

#	Article	IF	CITATIONS
37	<i>In Situ</i> Evaluation of Calcium Phosphate Nucleation Kinetics and Pathways during Intra- and Extrafibrillar Mineralization of Collagen Matrices. Crystal Growth and Design, 2016, 16, 5359-5366.	1.4	34
38	Microscopic Observations of Reductive Manganite Dissolution under Oxic Conditions. Environmental Science & amp; Technology, 2003, 37, 2363-2370.	4.6	33
39	Effects of Al/Si ordering on feldspar dissolution: Part II. The pH dependence of plagioclases' dissolution rates. Geochimica Et Cosmochimica Acta, 2014, 126, 595-613.	1.6	32
40	Classical and Nonclassical Nucleation and Growth Mechanisms for Nanoparticle Formation. Annual Review of Physical Chemistry, 2022, 73, 453-477.	4.8	32
41	Formation of Iron(III) (Hydr)oxides on Polyaspartate- and Alginate-Coated Substrates: Effects of Coating Hydrophilicity and Functional Group. Environmental Science & Technology, 2012, 46, 13167-13175.	4.6	31
42	The effects of initial acetate concentration on CO2–brine-anorthite interactions under geologic CO2 sequestration conditions. Energy and Environmental Science, 2011, 4, 4596.	15.6	30
43	Na+, Ca2+, and Mg2+in Brines Affect Supercritical CO2–Brine–Biotite Interactions: Ion Exchange, Biotite Dissolution, and Illite Precipitation. Environmental Science & Technology, 2013, 47, 191-197.	4.6	30
44	Nanoscale Chemical Processes Affecting Storage Capacities and Seals during Geologic CO ₂ Sequestration. Accounts of Chemical Research, 2017, 50, 1521-1529.	7.6	30
45	Supercritical CO2–brine induced dissolution, swelling, and secondary mineral formation on phlogopite surfaces at 75–95 °C and 75 atm. Energy and Environmental Science, 2012, 5, 5758.	15.6	29
46	Environmental and Geochemical Aspects of Geologic Carbon Sequestration: A Special Issue. Environmental Science & Technology, 2013, 47, 1-2.	4.6	29
47	MXene aerogel for efficient photothermally driven membrane distillation with dual-mode antimicrobial capability. Journal of Materials Chemistry A, 2021, 9, 22585-22596.	5.2	29
48	Antiscaling efficacy of CaCO ₃ and CaSO ₄ on polyethylene glycol (PEG)-modified reverse osmosis membranes in the presence of humic acid: interplay of membrane surface properties and water chemistry. Physical Chemistry Chemical Physics, 2017, 19, 5647-5657.	1.3	28
49	Does <i>Tert</i> -Butyl Alcohol Really Terminate the Oxidative Activity of [•] OH in Inorganic Redox Chemistry?. Environmental Science & Technology, 2021, 55, 10442-10450.	4.6	27
50	Structure of the Hydrated (101̄4) Surface of Rhodochrosite (MnCO3). Environmental Science & Technology, 2007, 41, 3918-3925.	4.6	25
51	Effects of organic ligands on supercritical CO2-induced phlogopite dissolution and secondary mineral formation. Chemical Geology, 2011, 290, 121-132.	1.4	25
52	Different Arsenate and Phosphate Incorporation Effects on the Nucleation and Growth of Iron(III) (Hydr)oxides on Quartz. Environmental Science & Technology, 2014, 48, 11883-11891.	4.6	25
53	Incorporating Nanoscale Effects into a Continuum-Scale Reactive Transport Model for CO ₂ -Deteriorated Cement. Environmental Science & Technology, 2017, 51, 10861-10871.	4.6	25
54	lonic Strength-Controlled Mn (Hydr)oxide Nanoparticle Nucleation on Quartz: Effect of Aqueous Mn(OH) ₂ . Environmental Science & Technology, 2016, 50, 105-113.	4.6	24

#	Article	IF	CITATIONS
55	Nanoscale <i>in situ</i> detection of nucleation and growth of Li electrodeposition at various current densities. Journal of Materials Chemistry A, 2018, 6, 4629-4635.	5.2	24
56	A Biosynthetic Hybrid Spidroin-Amyloid-Mussel Foot Protein for Underwater Adhesion on Diverse Surfaces. ACS Applied Materials & Interfaces, 2021, 13, 48457-48468.	4.0	24
57	Plagioclase Dissolution during CO ₂ –SO ₂ Cosequestration: Effects of Sulfate. Environmental Science & Technology, 2015, 49, 1946-1954.	4.6	23
58	Effects of Salinity-Induced Chemical Reactions on Biotite Wettability Changes under Geologic CO ₂ Sequestration Conditions. Environmental Science and Technology Letters, 2016, 3, 92-97.	3.9	23
59	Wollastonite carbonation in water-bearing supercritical CO2: Effects of water saturation conditions, temperature, and pressure. Chemical Geology, 2018, 483, 239-246.	1.4	23
60	Biotite Dissolution in Brine at Varied Temperatures and CO ₂ Pressures: Its Activation Energy and Potential CO ₂ Intercalation. Langmuir, 2012, 28, 14633-14641.	1.6	22
61	Fe ³⁺ Addition Promotes Arsenopyrite Dissolution and Iron(III) (Hydr)oxide Formation and Phase Transformation. Environmental Science and Technology Letters, 2016, 3, 30-35.	3.9	21
62	Microbial production of megadalton titin yields fibers with advantageous mechanical properties. Nature Communications, 2021, 12, 5182.	5.8	21
63	A mechanistic understanding of plagioclase dissolution based on Al occupancy and T–O bond length: from geologic carbon sequestration to ambient conditions. Physical Chemistry Chemical Physics, 2013, 15, 18491.	1.3	20
64	Photochemically-Assisted Synthesis of Birnessite Nanosheets and Their Structural Alteration in the Presence of Pyrophosphate. ACS Sustainable Chemistry and Engineering, 2017, 5, 10624-10632.	3.2	20
65	Structure-Dependent Interactions between Alkali Feldspars and Organic Compounds: Implications for Reactions in Geologic Carbon Sequestration. Environmental Science & Technology, 2013, 47, 150-158.	4.6	17
66	Fractal aggregation and disaggregation of newly formed iron(<scp>iii</scp>) (hydr)oxide nanoparticles in the presence of natural organic matter and arsenic. Environmental Science: Nano, 2016, 3, 647-656.	2.2	17
67	The Effects of Phosphonate-Based Scale Inhibitor on Brine–Biotite Interactions under Subsurface Conditions. Environmental Science & Technology, 2018, 52, 6042-6049.	4.6	17
68	Effects of Sulfate during CO ₂ Attack on Portland Cement and Their Impacts on Mechanical Properties under Geologic CO ₂ Sequestration Conditions. Environmental Science & Technology, 2015, 49, 7032-7041.	4.6	16
69	Salinity-Induced Reduction of Interfacial Energies and Kinetic Factors during Calcium Carbonate Nucleation on Quartz. Journal of Physical Chemistry C, 2019, 123, 14319-14326.	1.5	16
70	Sulfate-Controlled Heterogeneous CaCO ₃ Nucleation and Its Non-linear Interfacial Energy Evolution. Environmental Science & amp; Technology, 2021, 55, 11455-11464.	4.6	16
71	Effects of Phosphate, Silicate, and Bicarbonate on Arsenopyrite Dissolution and Secondary Mineral Precipitation. ACS Earth and Space Chemistry, 2020, 4, 515-525.	1.2	14
72	Cobalt Alters the Growth of a Manganese Oxide Film. Langmuir, 2006, 22, 2235-2240.	1.6	12

#	Article	IF	CITATIONS
73	Structural Match of Heterogeneously Nucleated Mn(OH) ₂ (s) Nanoparticles on Quartz under Various pH Conditions. Langmuir, 2016, 32, 10735-10743.	1.6	12
74	Photochemical reactions of dissolved organic matter and bromide ions facilitate abiotic formation of manganese oxide solids. Water Research, 2022, 222, 118831.	5.3	12
75	Distinctive Reactivities at Biotite Edge and Basal Planes in the Presence of Organic Ligands: Implications for Organic-Rich Geologic CO ₂ Sequestration. Environmental Science & Technology, 2015, 49, 10217-10225.	4.6	11
76	Effects of phosphate on biotite dissolution and secondary precipitation under conditions relevant to engineered subsurface processes. Physical Chemistry Chemical Physics, 2017, 19, 29895-29904.	1.3	11
77	Interfacial and Activation Energies of Environmentally Abundant Heterogeneously Nucleated Iron(III) (Hydr)oxide on Quartz. Environmental Science & Technology, 2020, 54, 12119-12129.	4.6	11
78	Co-effects of UV/H2O2 and natural organic matter on the surface chemistry of cerium oxide nanoparticles. Environmental Science: Nano, 2018, 5, 2382-2393.	2.2	10
79	The Role of Fe-Bearing Phyllosilicates in DTPMP Degradation under High-Temperature and High-Pressure Conditions. Environmental Science & Technology, 2018, 52, 9522-9530.	4.6	9
80	Cyclic strain enhances the early stage mineral nucleation and the modulus of demineralized bone matrix. Biomaterials Science, 2021, 9, 5907-5916.	2.6	9
81	Effects of MoS ₂ Layer Thickness on Its Photochemically Driven Oxidative Dissolution. Environmental Science & Technology, 2021, 55, 13759-13769.	4.6	9
82	Designing the crystalline structure of calcium phosphate seed minerals in organic templates for sustainable phosphorus management. Green Chemistry, 2018, 20, 534-543.	4.6	8
83	Redox chemistry of CeO ₂ nanoparticles in aquatic systems containing Cr(<scp>vi</scp>)(aq) and Fe ²⁺ ions. Environmental Science: Nano, 2019, 6, 2269-2280.	2.2	8
84	Supramolecular self-assembly of bacteriochlorophyll c molecules in aerosolized droplets to synthesize biomimetic chlorosomes. Journal of Photochemistry and Photobiology B: Biology, 2018, 185, 161-168.	1.7	7
85	Effects of Phosphonate Structures on Brine–Biotite Interactions under Subsurface Relevant Conditions. ACS Earth and Space Chemistry, 2018, 2, 946-954.	1.2	7
86	Pulsed Electrical Stimulation Enhances Body Fluid Transport for Collagen Biomineralization. ACS Applied Bio Materials, 2020, 3, 902-910.	2.3	7
87	Process-Specific Effects of Sulfate on CaCO ₃ Formation in Environmentally Relevant Systems. Environmental Science & Systems. Environmental Science & Society 2022, 56, 9063-9074.	4.6	7
88	Anorthite Dissolution under Conditions Relevant to Subsurface CO2 Injection: Effects of Na+, Ca2+, and Al3+. Environmental Science & amp; Technology, 2016, 50, 11377-11385.	4.6	6
89	Chapter 2 Anion Sorption Topology on Hematite: Comparison of Arsenate and Silicate. Developments in Earth and Environmental Sciences, 2007, , 31-65.	0.1	5
90	Engineering Calcium-Bearing Mineral/Hydrogel Composites for Effective Phosphate Recovery. ACS ES&T Engineering, 2021, 1, 1553-1564.	3.7	5

#	Article	IF	CITATIONS
91	Effects of Na ⁺ and K ⁺ Exchange in Interlayers on Biotite Dissolution under High-Temperature and High-CO ₂ -Pressure Conditions. Environmental Science & Technology, 2018, 52, 13638-13646.	4.6	4
92	Effects of sulfate on biotite interfacial reactions under high temperature and high CO ₂ pressure. Physical Chemistry Chemical Physics, 2019, 21, 6381-6390.	1.3	4
93	Kinetics of \hat{I}_{\pm} -MnOOH Nanoparticle Formation through Enzymatically Catalyzed Biomineralization inside Apoferritin. Crystal Growth and Design, 2017, 17, 5675-5683.	1.4	3
94	7. In situ Investigations of Carbonate Nucleation on Mineral and Organic Surfaces. , 2013, , 229-258.		2
95	Arsenite oxyanions affect CeO2 nanoparticle dissolution and colloidal stability. Environmental Science: Nano, 2021, 8, 233-244.	2.2	2
96	Frontiers and advances in environmental soil chemistry: a special issue in honor of Prof. Donald L. Sparks. Geochemical Transactions, 2020, 21, 6.	1.8	0